Selected papers presented at the Eleventh Annual Conference of the Materials Research Society of Serbia, YUCOMAT 2009

Gd_2O_3:Eu^{3+}/PMMA Composite: Thermal and Luminescence Properties

Ž. Antić, R. Krsmanović, M. Marinović-Cincović and M.D. Dramićanin*

Vinča Institute of Nuclear Sciences, P.O. Box 522, 110001 Belgrade, Serbia

In recent years there is an increasing interest in obtaining and investigating composite materials that comprise nanoparticles as fillers and polymers as matrix. Such composites may display combined features of both components, and sometimes even novel properties resulting from their mutual interactions. It is important that both unique size-dependent properties of nanoparticles and favorable properties of polymer material remain preserved in the composite. In this research we investigated the possibility of obtaining composite material using as polymer matrix poly (methyl methacrylate) — PMMA and Gd_2O_3:Eu^{3+} nanopowder as filler. Three samples, containing 1, 3 and 5 mass % of Gd_2O_3:Eu^{3+}, are prepared with a dispersion casting method. The composites exhibited characteristic red emission coming from the $^5D_0 \rightarrow {}^7F_2$ transition of Eu^{3+} ion in Gd_2O_3:Eu^{3+}. The observed lifetime values, around 1.1 ms, are quite high and suggest successful encapsulation of dopant ions in polymer through gadolinium oxide host. Experimental intensity parameters, transition rates and quantum efficiency of the $^5D_0$ emission are calculated from emission spectra using Judd–Ofelt theory. Influence of Gd_2O_3:Eu^{3+} filler on the modification of glass transition and thermo-degradable properties of the polymer matrix is also investigated. Thermal analyses give evidence of unchanged thermal stability of polymer phase in the composites.

PACS numbers: 81.20, 32.50, 42.70.J.

1. Introduction

The general class of nanocomposite organic/inorganic materials is a fast growing area of research which is generating many exciting new materials with novel properties. The latter can derive by combining properties from the parent constituents into a single material. There is also the possibility of new properties which are unknown in the parent constituent materials.

Rare-earth ion doped nanocrystals dispersed in a transparent polymer medium are of special interest as potential optoelectronic materials that may find applications as light emitters for integrated optoelectronic and photonic circuits. This type of nanocomposite provides phosphorescent material with optimized local environment for both optical and thermal stability [1–3].

Among broad variety of available polymers, poly (methyl methacrylate), (PMMA), with its outstanding mechanical, chemical and physical properties, represents a particularly suitable embedding medium for nanoscopic inorganic fillers. PMMA possesses a unique combination of excellent optical properties (clarity, transparency from the near UV to the near IR) and chemical inertness, some good mechanical properties, thermal stability, electrical properties, safety, weather resistance, formability, and easy shaping [4]. A further advantage of PMMA relies on its large availability and easy preparation [5]. PMMA embedding inorganic or organically modified inorganic particles has been cast into films to yield enhanced functional properties such as photoconductivity [6], photoinduced charge-transfer [7], nonlinear optical properties [8], photoluminescence [9, 10], mechanical [11] and magnetic properties [12].

In this paper we analyzed phosphorescence and thermal properties of nanocomposites prepared from PMMA and Gd_2O_3:Eu^{3+}. Phosphorescence emission, transition rates and quantum efficiency of nanocomposites are compared to those obtained with Gd_2O_3:Eu^{3+} nanopowder, while temperatures of glass transitions and nanocomposite thermal stabilities are compared to those found for pure PMMA.

2. Experimental

In the first stage of the experiment we synthesized nanopowders of Gd_2O_3 doped with 3 at.% Eu^{3+}. Oxides of gadolinium and europium (all Alfa Aesar 99.9%) were used as the starting materials, while polyethylene glycol with average molecular weight 20000 (PEG 20000, Alfa Aesar) served as fuel to provide the combustion reaction. Water solutions of stoichiometric quantities of Gd and Eu-nitrate were prepared by dissolving 1 g of Gd_2O_3 and 0.0726 g of Eu_2O_3 in hot nitric acid. In so obtained

* corresponding author; e-mail: dramican@vinca.rs

solution PEG was added in 1:1 mass ratio to used oxides. After forming metal-PEG solution and stirring at 80 °C metal-PEG solid complex was formed. Complex is combusted at 800 °C in air and calcinated at the same temperature for 2 h to form nanopowder samples.

The polymer used as a host material for phosphor nanoparticles was poly (methyl methacrylate). Nanocomposites of PMMA/Gd_2O_3:Eu^{3+} were prepared by dispersing appropriate amount of Gd_2O_3:Eu^{3+} (1, 3 and 5 mass % to PMMA) in xylene solution of commercially available Diakon CMG 314 V PMMA (average molecular weight $M_w = 90000$, polydispersity index $M_w/M_n = 2.195$). Initially, Gd_2O_3:Eu^{3+} nanopowders were dispersed in xylene (Aldrich), by stirring with a high sheer rate for 18 h, followed by treatment in an ultrasonic bath for 3 h. PMMA was dissolved in the same amount of xylene. After that, the slurry containing phosphor nanoparticles was added to the polymer solution and the mixture was pured out on a flat surface. The solvent was removed by evaporation under ambient conditions. After evaporation of solvent, content of nanophosphors in PMMA matrices was 1, 3 and 5 mass %.

Structure and morphology Gd_2O_3:Eu^{3+} nanoparticles are presented in Ref. [13]. In brief, X-ray diffraction (XRD) measurements showed cubic structure (206 space group $Ia\bar{3}$) with average particle size of around 30 nm. Transmission electronic microscopy (TEM) analysis showed that particles have size in the range of 20–50 nm.

Photoluminescence emission spectra and lifetime measurements were done at room temperature, on the Fluorolog-3 Model FL3-221 spectroflurometer system (HORIBA Jobin–Yvon). For emission spectra measurements a 450 W Xenon lamp and TBX detector were used. For the lifetime measurements 150 W pulsed Xenon lamp and TBX single photon timing system were utilized.

Differential scanning calorimetry (DSC) measurements of PMMA and PMMA/Gd_2O_3:Eu^{3+} nanocomposites were performed on a Perkin–Elmer DSC-2 instrument in the temperature range from 50 to 150 °C. The heating rate was 20 °C/min. In order to prepare samples with the same thermal history, samples were heated prior to measurements above the glass transition temperature and then cooled down (heating and cooling rates were 20 °C/min). The thermal stability of pure PMMA and the PMMA/Gd_2O_3:Eu^{3+} samples was investigated by non-isothermal thermo-gravimetric analysis (TG) using a SETARAM SETSYS Evolution-1750 instrument. The measurements were conducted at a heating rate of 10 °C/min in a dynamic argon atmosphere (flow rate 20 cm^3/min) in the temperature range from 30 to 500 °C.

3. Results and discussion

3.1. Photoluminescence measurements

In investigated composites luminescence emission is provided via electronic transitions in Eu^{3+} dopant ion. This emission is characteriscs of this ion and is influenced by chemical surroundings. Emission spectra ($\lambda_{ex} = 467$ nm) of pure Gd_2O_3:Eu^{3+} and of PMMA/Gd_2O_3:Eu^{3+} (1, 3 and 5 mass %) composite are presented in Fig. 1. In this figure characteristic emissions [14] associated to $^5D_0 \rightarrow {}^7F_J$ ($J = 0$, 1, 2, 3 and 4) spin forbidden f–f transitions can be observed in all cases. At 580 nm one can notice emission from $^5D_0 \rightarrow {}^7F_0$ transition. The $^5D_0 \rightarrow {}^7F_1$ transition is the parity-allowed magnetic dipole transition ($\Delta J = 1$) and its intensity is not influenced by the host. For this transition three distinct emission lines situated 588, 592 and 598 nm can be observed ($2J + 1 = 3$). The $^5D_0 \rightarrow {}^7F_2$ electric dipole transition ($\Delta J = 2$) is very sensitive to the local environment around Eu^{3+}, and its intensity depends on the symmetry of the crystal field around the europium ion [15]. Emissions coming from $^5D_0 \rightarrow {}^7F_3$ and $^5D_0 \rightarrow {}^7F_4$ transitions can be noticed at around 651 and 708 nm, respectively.

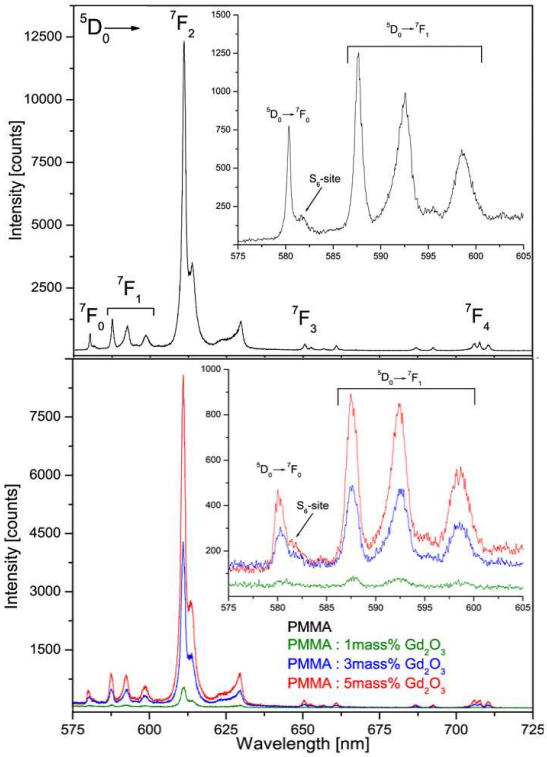

Fig. 1. Emission spectra of pure Gd_2O_3:Eu^{3+} (top) and PMMA/Gd_2O_3:Eu^{3+} (bottom) composite ($\lambda_{ex} = 467$ nm).

Inserts in Fig. 1 are given in order to closely examine $^5D_0 \rightarrow {}^7F_1$ and $^5D_0 \rightarrow {}^7F_0$ transitions. One can observe a peak originating from $^5D_0 \rightarrow {}^7F_0$ transition of Eu^{3+} located in C_2 site at around and from $^5D_0 \rightarrow {}^7F_1$ transition of Eu^{3+} located in S_6 site at around. Both of them are in good agreement with the literature data [14]. C_2 and S_6 sites differ from each other in the position of rare earth ion relative to oxygen vacancy. Due to presence of inversion symmetry for S_6 site only the magnetic dipole-induced transitions may occur ($\Delta J = 0$ or 1, but $0 \rightarrow 0$ transition forbidden) [16, 17]. Therefore in luminescence

spectra of Eu^{3+} doped cubic sesquioxides only one line with very low intensity originates from Eu^{3+} ions in S_6 sites, and practically all observed transitions comes from Eu^{3+} ions in the C_2 sites, Table I. Stark components of the $^7F_1$ manifold are also clearly visible.

Figure 2 shows the results of the emission lifetime measurements (λ_{ex} = 467 nm, λ_{em} = 611 nm) of pure Gd_2O_3:Eu^{3+} powder and PMMA/Gd_2O_3:Eu^{3+} composite at room temperature. The luminescence decay profile could be fitted by a single-exponential function. The calculated lifetime values are given in Table II. Obtained rather high values are characteristic of europium species with low non-radiative energy transfer probability that is very favorable for further applications.

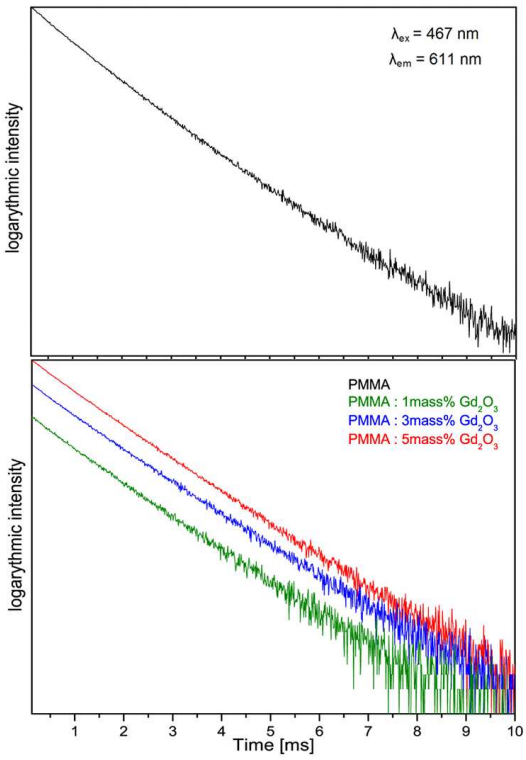

Fig. 2. Luminescence decay profiles for pure Gd_2O_3:Eu^{3+} (top) and PMMA/Gd_2O_3:Eu^{3+} (bottom) composite at room temperature (λ_{ex} = 467 nm, λ_{em} = 611 nm).

3.2. Experimental intensity parameters, transition rates and quantum efficiency of the $^5D_0$ emission

The spectra of trivalent lanthanide in solution or crystal lattice arise from forbidden transitions within the $4f^n$ — configuration to which the Judd–Ofelt (JO) [18, 19] theory has been successfully applied in quantitative determination of its optical properties. The application of JO theory to the quantitative analysis of Eu^{3+} emissive properties in matrix is nicely presented by Werts et al. [20], and can be summarized as follows.

Radiative relaxation from an excited state ΨJ of a lanthanide ion usually occurs to various lower lying states $\Psi' J'$, giving rise to several lines in the emission spectrum. The red luminescence of Eu^{3+} is a result of transitions from its $^5D_0$ state to all of the lower lying ^7F_J levels. According to JO theory the spontaneous emission probability, A, of the transition $\Psi J \rightarrow \Psi' J'$ is related to its dipole strength according to following equation:

$$A(\Psi J, \Psi' J') = \frac{64\pi^4 \nu_{\text{avg}}^3}{3h(2J+1)} \times \left[\frac{n(n^2+2)^2}{9} D_{\text{ED}} + n^3 D_{\text{MD}}\right] \quad (1)$$

Where ν_{avg} is the average transition energy in cm^{-1}, h is Planck constant (6.63×10^{-27} erg s), $2J+1$ is the degeneracy of the initial state (1 for $^5D_0$). D_{ED} and D_{MD} are the electric and magnetic dipole strength (in [esu^2] [cm^2]), respectively. The factors containing medium's refractive index n result from local field corrections that convert the external electromagnetic field into an effective field at the location of the active center in the dielectric medium.

The transitions from $^5D_0$ to $^7F_{0,3,5}$ are forbidden both in magnetic and induced electric dipole schemes (D_{ED} and D_{MD} are zero). The transition to $^7F_1$ ($J' = 1$) is the only magnetic dipole transition, and has no electric dipole contribution. Magnetic dipole transitions in lanthanide ions are practically independent of the ion's surroundings, and can be well calculated by theory ($D_{\text{MD}} = 9.6\times10^{-42}$ esu^2 cm^2 $= 9.6\times10^{-6}$ debye^2) [20].

The remaining transitions ($J' = 2$, 4, 6) are purely of induced electric dipole nature, and the strength of all induced dipole transitions can be calculated on basis of only three phenomenological parameters Ω_λ (JO parameters) using following equation

$$D_{\text{ED}} = e^2 \sum_{\lambda=2,4,6} \Omega_\lambda \left| \left\langle \Psi J \left\| U^{(\lambda)} \right\| \Psi' J' \right\rangle \right|^2, \quad (2)$$

Where e stands for elementary charge e and $|\langle \Psi J \| U^{(\lambda)} \| \Psi' J' \rangle|^2$ are the squared reduced matrix elements whose values are independent of the chemical environment of the ion. For the case of Eu^{3+} these values are given in Refs. [20] (Table I).

The R_{02} intensity parameter, defined as the ratio between the intensities of the $^5D_0 \rightarrow {}^7F_0$ and $^5D_0 \rightarrow {}^7F_2$ transitions, gives information on the J-mixing effect associated with the $^5D_0 \rightarrow {}^7F_0$ transition. This effect is mainly due to the mixing between the $^7F_2$ manifold and the $^7F_0$ level, through the rank two components of the ligand field.

One can observe from Table I and Eq. (2) that each electric dipolar $^5D_0 \rightarrow {}^7F_{2,4,6}$ transition depends only on one squared reduced matrix element. This unique feature for the Eu^{3+} ion facilitates the determination of JO parameters from the emission spectra. Thus, the experimental intensity parameter Ω_λ can be calculated from the ratio of the intensity of the $^5D_0 \rightarrow {}^7F_\lambda$ (λ = 2, 4 and 6) transitions, $\int I_\lambda(\nu)\,\mathrm{d}\nu$, to the intensity of the $^5D_0 \rightarrow {}^7F_1$ transition, $\int I_1(\nu)\,\mathrm{d}\nu$ as follows:

$$\Omega_\lambda = \frac{D_{\mathrm{MD}}\nu_1^3}{\mathrm{e}^2\nu_\lambda^3}\frac{9n^3}{n(n^2+2)^2\left|\left\langle \Psi J \left\| U^{(\lambda)} \right\| \Psi' J' \right\rangle\right|^2} \times \frac{\int I_\lambda(\nu)\,\mathrm{d}\nu}{\int I_1(\nu)\,\mathrm{d}\nu}\,. \quad (3)$$

Then, probabilities of each spontaneous emission (radiative rates) can be obtained from Eqs. (1) and (2) using calculated Ω_λ parameters. Total radiative rate, A_{R}, defined as sum all radiative rates, can be further used to evalute nonradiative rate, A_{NR}, and emission quantum efficiency, η, (ratio between number of photons emitted by the Eu^{3+} ion to those absorbed by the Eu^{3+} ion) in the following way:

$$A_{\mathrm{NR}} = 1/\tau - A_{\mathrm{R}}\,, \quad \eta = A_{\mathrm{R}}/(A_{\mathrm{R}} + A_{\mathrm{NR}}) \quad (4)$$

where τ stands for the emission lifetime.

Results of calculation are given in Table II (refraction index is taken from dispersion relation given by [21]. Since the emission band for $^5D_0 \rightarrow {}^7F_6$ transition, centered at around 810 nm, could not be detected due to limitation of measurement spectral range, we can only determine the value of Ω_2 and Ω_4. However, it has been shown that the influence of Ω_6 can be neglected in determination of radiative properties of Eu^{3+} ions [22, 23].

TABLE I

Squared reduced matrix elements used for calculation of dipole strengths of the allowed induced ED transitions in the emission spectrum of Eu^{3+}, taken from [19].

$^5D_0 \rightarrow$	$\lvert\langle \Psi J \lVert U^{(2)} \rVert \Psi' J' \rangle\rvert^2$	$\lvert\langle \Psi J \lVert U^{(4)} \rVert \Psi' J' \rangle\rvert^2$	$\lvert\langle \Psi J \lVert U^{(6)} \rVert \Psi' J' \rangle\rvert^2$
$^7F_2$	0.0032	0	0
$^7F_4$	0	0.0023	0
$^7F_6$	0	0	0.0002

TABLE II

$\Omega_{2,4}$ parameters, spontaneous emission probability (A_1, A_2, A_4), radiative transition rates (A_{R}), nonratiative rate (A_{NR}), experimental lifetime (τ), emission quantum efficiency (η) and intensity parameter (R_{02}) of Gd_2O_3:Eu^{3+} and PMMA/Gd_2O_3:Eu^{3+} composites.

	Gd_2O_3:Eu^{3+} powder	PMMA/1 mass % Gd_2O_3:Eu^{3+}	PMMA/3 mass % Gd_2O_3:Eu^{3+}	PMMA/5 mass % Gd_2O_3:Eu^{3+}
Ω_2 [10^{-20} cm^2]	10.37	5.84	4.83	9.21
Ω_4 [10^{-20} cm^2]	3.09	1.47	3.12	2.08
A_1 [s^{-1}]	98.6	47.6	47.6	47.6
A_2 [s^{-1}]	637.7	159.4	131.6	251.2
A_4 [s^{-1}]	85.6	18.0	38.4	25.6
A_{R} [s^{-1}]	821.9	225.0	217.6	324.4
A_{NR} [s^{-1}]	32.8	718.4	744.0	610.2
τ [ms]	1.17	1.06	1.04	1.07
η [%]	96.2	23.9	22.6	34.7
R_{02}	0.0179	0.0696	0.0855	0.0303

3.3. Thermal analysis

The glass transition behavior of the PMMA and nanocomposites was investigated by DSC. The heat capacity curves of the pure PMMA and PMMA/Gd_2O_3:Eu^{3+} nanocomposites are shown in Fig. 3. A shift in the slope of the heat capacity curves towards higher temperatures was observed after incorporation of Gd_2O_3:Eu^{3+} in to the PMMA matrix. This slope, of course, corresponds to the glass transition temperature (T_{g}) of the polymer. It should be emphasized that the glass transition is not a true phase transition since the derivative of the heat capacity can be a continuous function of temperature. The different segmental motions lead to the glass transition spectrum.

The values of the glass transition temperature were taken as the midpoint of the glass event. The obtained values for pure PMMA and PMMA/Gd_2O_3:Eu^{3+} nanocomposites are listed in Table III. One can notice that glass transition temperatures of the PMMA/Gd_2O_3:Eu^{3+} composites (97, 98 and 100 ℃) are higher compared to value for pure PMMA (95 ℃)

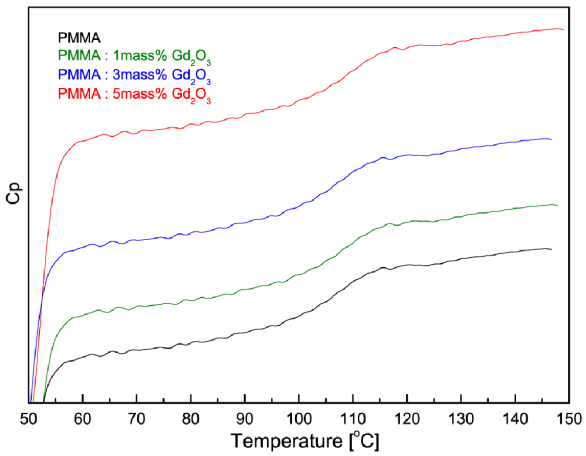

Fig. 3. The heat capacity curves of the pure PMMA and PMMA/Gd_2O_3:Eu^{3+} nanocomposites with 1%, 3% and 5 mass % Gd_2O_3:Eu^{3+}.

TABLE III

Glass transition temperatures of PMMA and PMMA/Gd_2O_3:Eu^{3+} nanocomposites with 1%, 3% and 5 mass % Gd_2O_3:Eu^{3+}.

Sample	T_g [°C]
PMMA	95
PMMA: 1 mass % Gd_2O_3:Eu^{3+}	97
PMMA: 3 mass % Gd_2O_3:Eu^{3+}	98
PMMA: 5 mass % Gd_2O_3:Eu^{3+}	100

The observed effect can be explained as a consequence of decreased molecular mobility of the PMMA chains due to adhesion of polymer segments onto the surface of Gd_2O_3:Eu^{3+}. Because of that, PMMA/Gd_2O_3:Eu^{3+} nanocomposites glass transition is slightly improved in respect to pure PMMA. The broadening of the glass transition region for the PMMA/Gd_2O_3:Eu^{3+} was also observed. If we assume that the T_g corresponds to the motion of segments with some average length, then the presence of filler particles alters the distribution of segmental lengths and consequently induce changes in the glass transition region.

The thermal stability of the PMMA and PMMA/Gd_2O_3:Eu^{3+} samples were examined by non-isothermal thermo-gravimetry. It is known that PMMA thermally decomposes by depolymerization [24]. The thermal stability of free radically polymerized PMMA is significantly affected by the presence of unsaturated end groups and head-to-head bonds obtained during termination by disproportionation and combination, respectively. The thermal degradation of PMMA occurs in three stages, characterized by three minima in the differential thermal gravimetry (DTG) curve at about 180, 300 and 380 °C at a heating rate of 10 °C/min [25–28]. These stages have been attributed to different modes of initiation of depolymerization. The first peak corresponds to depolymerization initiated by the scission of the weak head-to-head bonds and the second one corresponds to depolymerization initiated by the unsaturated vinyl chain ends. The third peak corresponds to depolymerization initiated by random main chain scission.

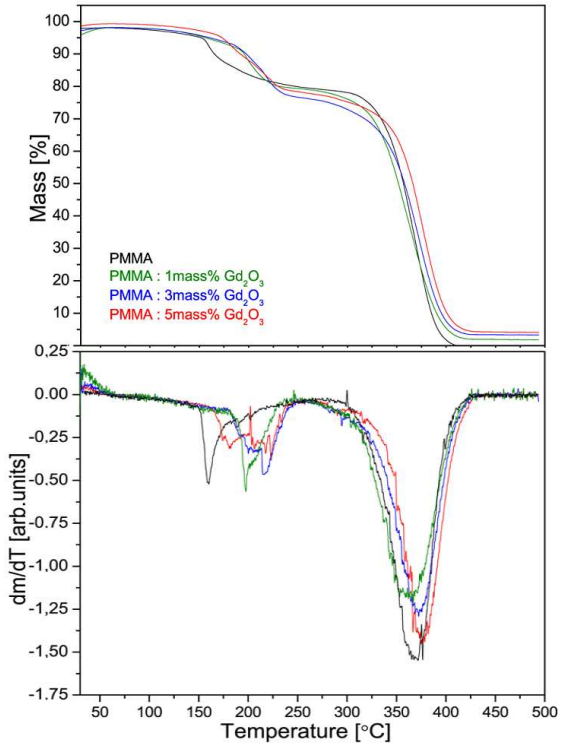

Fig. 4. TG (top) and DTG (bottom) curves of pure PMMA and PMMA/Gd_2O_3:Eu^{3+} composites with 1%, 3% and 5 mass % obtained under argon atmosphere and at heating rate of 10 °C/min.

Thermal gravimetry (TG) and differential thermal gravimetry (DTG) curves obtained for the pure PMMA and PMMA/Gd_2O_3:Eu^{3+} samples in argon atmosphere are shown in Fig. 4. The thermal degradation of PMMA and PMMA/Gd_2O_3:Eu^{3+} samples occur in two stages, and their TG and DTG curves are very similar. Peak position temperatures of DTG curves for PMMA and PMMA/Gd_2O_3:Eu^{3+} composites with 1%, 3% and 5 mass % obtained in argon atmosphere are shown in Table IV. For broad peak that corresponds to PMMA/5 mass % Gd_2O_3:Eu^{3+} peak position temperature was taken at the peak midpoint.

The first DTG peak which corresponds to depolymerization initiated by the scission of the weak head-to-head bonds not only shifts to the higher temperatures but also becomes broader or even splits into several bands for the composite samples (Table IV, T_{min1}). This could not be attributed either to depolymerisation initiated by the scission of the weak head-to-head bonds or depolymerisation initiated by unsaturated vinyl ends. It can be as-

TABLE IV

Peak position temperatures of DTG curves for investigated samples obtained in argon atmosphere.

Sample	T_{min1} [°C]	T_{min2} [°C]
Pure PMMA	160	369
PMMA: 1 mass % Gd_2O_3:Eu^{3+}	196	370
PMMA: 3 mass % Gd_2O_3:Eu^{3+}	217	373
PMMA: 5 mass % Gd_2O_3:Eu^{3+}	222	375

sumed that it was caused by the removal of volatile low molar mass components generated during the preparation of composites. The most intense DTG peak (T_{min2}) for all investigated samples is peak which corresponds to depolymerization initiated by random chain scission at 369 °C (PMMA) and at 370, 373, 375 °C (composites with 1%, 3% and 5 mass % of Gd_2O_3:Eu^{3+}). Samples do not contain peak at 300 °C which corresponds to depolymerization initiated by the unsaturated vinyl chain ends. The obtained results indicate that the incorporation of Gd_2O_3:Eu^{3+} preserves or even slightly improves the thermal stability of the PMMA matrix.

4. Conclusions

The PMMA/Gd_2O_3:Eu^{3+} composites exhibit characteristic red phosphorescence from electronic transitions in trivalent europium ions. Quite good quantum efficiencies, from 23% to 35%, are achieved, suggesting promising applications for these composites. From presented data one may conclude that the optical emission, the main function of inorganic phosphor filler, is completely preserved in prepared composites. Also, thermal analyses give evidence of unchanged or even slightly improved, thermal stability of polymer phase in composites.

Acknowledgments

Authors acknowledge the support of the Ministry of Science of the Republic of Serbia (project number 141026).

References

[1] Y. Changhao, D. Hongli, G. Chunfang, L. Ping, W. Wenxuan, Z. Ming, Q. Guanming, *J. Rare Earth.* **25**, 20 (2007).

[2] Q. Shangguan, X. Cheng, *J. Rare Earth.* **25**, 469 (2007).

[3] Q. Guanming, Y. Changhao, G. Chunfang, W. Wenwuan, Z. Ming, *J. Rare Earth.* **25**, 5 (2007).

[4] H.F. Mark, N.M. Bikales, C.G. Overberger, G. Menges, in: *Encyclopedia of polymer science and technology*, John Wiley and Sons, New York 1985.

[5] S. Gross, D. Camozzo, V. Di, L. Noto, E. Armelao, Tondello, *Eur. Polym. J.* **43**, 673 (2007).

[6] A. Thander, B. Mallik, *Solid State Commun.* **111**, 341 (1999).

[7] A. Thander, B. Mallik, *Chem. Phys. Lett.* **330**, 521 (2000).

[8] I. Lee, Y. Niidome, T. Matsuo, S. Yamada, *Anal. Sci.* **13**, 343 (1997).

[9] K. Rawlins, A. Lees, S. Fuerniss, K. Papathomas, *Chem. Mater.* **8**, 1540 (1996).

[10] S.C. Farmer, T.E. Patten, *Chem. Mater.* **13**, 3920 (2001).

[11] B.J. Ash, D.F. Rogers, C.J. Wiegand, L.S. Schadler, R.W. Siegel, B.C. Benicewicz, T. Apple, *Polym. Composite* **23**, 1014 (2004).

[12] A. Horikawa, K. Yamaguchi, M. Inoue, T. Fujii, K. Arai, *Mater. Sci. Eng.* **217**, 348 (1996).

[13] M. Marinović-Cincović, Ž. Antić, R. Krsmanović, M. Mitrić, M.D. Dramićanin, *J. Optoelectron. Adv. M. — Symposia* **1**, 54 (2009).

[14] Ž. Andrić, M.D. Dramicanin, M. Mitrić, V.Jokanović, A. Bessiere, B. Viana, *Opt. Mater.* **30**, 1023 (2008).

[15] W.M. Yen, S. Shionoya, H. Yamamoto, in: *Phosphor handbook*, CRC Press, Boca Raton, ch. 3.

[16] E. Zych, *J. Phys. Condens. Mat.* **14**, 5637 (2002).

[17] E. Zych, J. Trojan-Piegza, *J. Lumin.* **122-123**, 335 (2007).

[18] B.R.Judd, *Phys. Rev.* **127**, 750 (1962).

[19] G.S. Ofelt, *J. Chem. Phys.* **37**, 511 (1962).

[20] M.H.V. Werts, R.T.F.Jukes, J.W. Verhoeven, *Phys. Chem. Chem. Phys.* **4**, 1542 (2002).

[21] S.N. Kasarova, N.G. Sultanova, C.D. Ivanov, I.D. Nikolov, *Opt. Mater.* **29**, 1481 (2007).

[22] R. Balakrishnaiah, R. Vijaya, P. Babu, C.K. Jayasankar, M.L.P. Reddy, *J. Non-Cryst. Solids* **353**, 1397 (2007).

[23] K. Marimuthu, R.T. Karunakaran, S. Surendra, G. Babu, S. Muralidharan, C.K. Arumugam, Jayasankar, *Sol. State Sci.* **11**, 1297 (2009).

[24] I.C. McNeill, *Eur. Polym. J.* **4**, 21 (1968).

[25] T. Kashiwagi, A. Inaba, J.E. Brown, K. Hatada, T. Kitayama, E. Masuda, *Macromolecules* **19**, 2160 (1986).

[26] I.G. Popovic, L. Katsikas, H. Weller, *Polym. Bull.* **32**, 597 (1994).

[27] L. Katsikas, J.S. Velickovic, H. Weller, I.G. Popovic, *J. Therm. Anal.* **49**, 317 (1997).

[28] T. Kashiwagi, T. Hirata, J.E. Brown, *Macromolecules* **18**, 131 (1985).